Efficient Multi-keV Underdense Laser-Produced Plasma Radiators

C. A. Back,[1] J. Grun,[2] C. Decker,[1] L. J. Suter,[1] J. Davis,[3] O. L. Landen,[1] R. Wallace,[1] W. W. Hsing,[1] J. M. Laming,[2]
U. Feldman,[2] M. C. Miller,[1] and C. Wuest[1]

[1]*Lawrence Livermore National Laboratory, L-21, P.O. Box 808, Livermore, California 94551*
[2]*Naval Research Laboratory, 4555 Overlook Ave., SW, Washington, D.C. 20375*
[3]*Alme & Associates, 6020 Richmond Highway, Alexandria, Virginia 22303*
(Received 2 June 2000; published 12 December 2001)

Novel, efficient x-ray sources have been created by supersonically heating a large volume of Xe gas. A laser-induced bleaching wave quickly ionizes the high-Z gas, and the resulting plasma emits x rays. This method significantly improves the production of hard x rays because less energy is lost to kinetic energy and sub-keV x rays. The conversion efficiency of laser energy into L-shell radiation between 4–7 keV is measured at ∼10%, an order of magnitude higher than efficiencies measured from solid disk targets. This higher flux enables material testing and backlighting in new regimes and scales well to future high-powered lasers.

X-ray sources with high multi-keV conversion efficiency (CE) are important to laser fusion and a multitude of applications [1], including radiography of crystals and plasmas, fluorescence techniques, and material testing. Extensive research on laser-heated disks has shown that sub-keV x rays are predominantly generated in an ablated conversion layer, while multi-keV x rays are produced in the expanding, lower density nonlocal thermodynamic equilibrium (non-LTE) plasma [2–4].

Unfortunately, steep material gradients in these plasmas make it difficult to optimize the temperature and density conditions for multi-keV (hard) x-ray production [5]. Past disk experiments measured multi-keV CE <1% [4,6,7] and data are low compared to predictions, especially for those at later intensities >10^{15} W/cm^2. Although the electron heat flux limiter in the plasma model can be adjusted to match the data, the discrepancy remains unexplained and is a stumbling block to developing brighter sources with higher photon energies.

In this Letter we present data showing the highest multi-keV CE to date in laser-produced plasmas. This research significantly extends the accessible photon energy ($h\nu > 4$ keV) and utility of multi-keV sources for new applications. Such sources are critically needed to probe the denser plasmas expected in experiments at the National Ignition Facility (NIF) [8]. They also show promise as high-brightness, low-debris sources in the 4–10 keV energy range, where there is a lack of suitable sources for specialized material testing applications [9]. In addition, this research enables controlled studies of non-LTE processes because the initial conditions of the plasma can be well characterized.

To improve the multi-keV CE, we have developed "underdense" radiators. These sources are created by laser irradiating a confined gas. The term "underdense" means that the initial ionized electron density, n_e, is less than the critical density for the laser, $n_c = 1.1 \times 10^{21}/\lambda_L^2$ cm^{-3}, where λ_L is the laser wavelength in μm. When $n_e < n_c$,

laser absorption occurs predominately by inverse bremsstrahlung and a supersonic heat wave propagates in the gas. This research has increased x-ray CE by an order or magnitude and represents a new pathway for the development of efficient, large-area, multi-keV x-ray sources.

All the experiments were performed on the Nova laser using 35.6 ± 3.2 kJ in ten beams of 0.35 μm light delivered in a 2-ns-long square pulse. Figure 1(a) shows a schematic of the target and the laser irradiation. Five beams enter through laser entrance holes (LEH) from each side of a cylindrical Be enclosure, or "can," containing 1 atm of high-Z gas. Opposite beams produce overlapping spots on the inside wall to irradiate as large a volume as possible. The intensity varies from 2×10^{15} W/cm^2 at the LEH to 4×10^{14} W/cm^2 at the cylindrical Be wall. The path length through the gas was 1.3 mm long from the LEH to the wall.

The cylindrical enclosure was 2 mm in diameter and 1.6 mm long. It was constructed from a 100-μm-thick Be tube, capped on either end by 50-μm-thick Be washers. The LEHs were 1.5 mm in diameter and covered with 3500 Å of polyimide ($C_{16}H_6N_2O_4$) to confine the gas. The enclosure itself was designed to have two functions: (i) to serve as a pressure vessel to contain the gas, and (ii) to provide hydrodynamic tamping of the Xe gas so that the
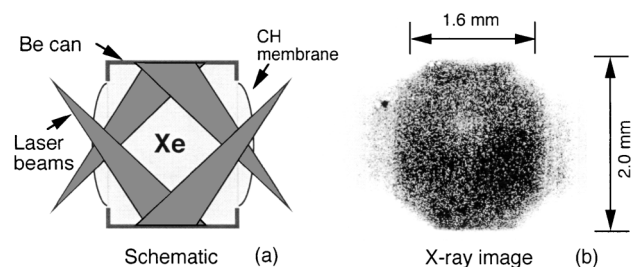
FIG. 1. (a) Schematic of a gas-filled target. Laser beams enter each side in a cylindrically symmetric geometry. (b) 2D x-ray image at 1.8 ns for $h\nu > 4$ keV.

target does not disassemble like gas-filled balloons, called "gas bags," used in other plasma studies [10].

The gas was a mixture of 80% Xe and 20% Kr. Xe, whole L-shell emission is in the 4–7 keV range, was the primary gas of interest. Kr was present to act as a spectroscopic tracer [4]. Simulations and x-ray image data confirmed that the tracer gas did not perturb the hydrodynamics.

The use of a *gas-filled* target is important because the initial density, $\rho \sim 0.003$ g/cm^3, could be strictly controlled to ensure that an underdense plasma is formed. Furthermore, the radiator size is well defined by the walls of the enclosure. The initial density of Xe is measured with high accuracy by transducers that monitor the gas pressure. When ionized to a charge state of 44, the nominal 1 atm pressure translates to $n_e \sim 1 \times 10^{21}$ cm^{-3}, which is $\sim 0.1 n_c$. In the series of five experiments discussed here target pressures averaged 1.05 atm $\pm 5\%$ at shot time.

X-ray CE measurements of L-shell emission are not well documented in the literature. Therefore, to conclusively demonstrate the improved efficiency of supersonic heating, we also performed four experiments on conventional ablatively heated cesium iodide CsI disk targets for comparison. Cs and I bracket Xe in the periodic table and serve as a substitute for a solid Xe target which would have required cryogenic cooling.

A comprehensive set of instruments diagnose the Xe plasma through the Be wall. The most important were Bragg crystal spectrometers and a set of seven x-ray diodes (XRDs) which measures multi-keV absolute flux. The two spectrometers, located at 25° and 68° from the cylindrical axis, provide time-integrated spectra with ~ 6 mÅ spectral resolution. The XRDs, filtered with Be, Fe, Ti, V, and Zr, measure the time-resolved flux in broadband spectral channels.

Different diagnostics measured other characteristics of the x-ray source. Gated pinhole cameras provided two-dimensional (2D) x-ray images filtered for x rays greater than 4 keV [see Fig. 1(b)]. X-ray streak cameras equipped with Bragg crystals measured the $n = 3-2$ emission resolved in time. Filtered radiochromic x-ray film packs were fielded at different angles in the target chamber to measure the isotropy of the emission. In addition, ten x-ray diodes (Dante) measured the thermal x-ray emission [11].

The Bragg crystal spectrometers record spectrally resolved absolute flux onto Kodak direct exposure film. A set of Ti, V, and Al filters on each piece of film enabled weak and strong line intensities to be recorded on a single shot with a dynamic range of 20. In Fig. 2, the Xe and CsI spectra are shown together with the CsI vertically offset -0.5. The time-integrated spectrum is spectrally integrated over the 4–7 keV energy range to obtain the total energy emitted by L-shell radiation from the plasma. The total L-shell energy is then divided by the laser energy to give the multi-keV x-ray CE.

The raw spectroscopic data are converted to source fluence by converting film density to exposure [12] and then
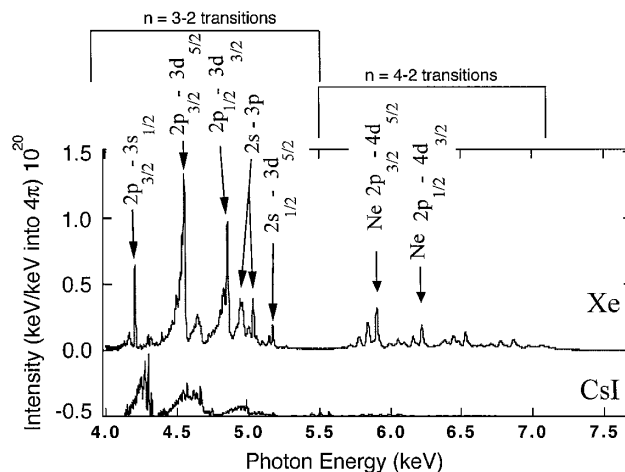
FIG. 2. Spectra from Bragg crystal spectrometers. The CsI from a disk target is multiplied 10× and offset -0.5 relative to the underdense Xe target.

correcting for the geometry, filters, and crystal reflectivities. The thin filters were laboratory calibrated and checked *in situ* for self-consistency. The reflectivities were measured, using a Manson source with a Ti anode (4.7 keV) that is well matched to the peak Xe emission. This calibration is accurate to 8% and was particularly important to the CE because theoretical reflectivities can vary widely depending on the assumed crystal structure (perfect or mosaic). This calibration has been cross-checked in the 2–4 keV range with the Dante diagnostic on gas-bag targets [13]. The best crystals showed 5% variations in reflectivity across the width of the crystal utilized; crystals with >10% variations were rejected. At the upper energy end of the spectrum, hard x rays penetrate deeper into the crystal and errors of up to 25% can be expected. However, $\sim 80\%$ of the L-shell emission is emitted below 6 keV; therefore the larger error at higher photon energies is compensated by a smaller weighting factor on its contribution to the measurement.

X-ray diodes provide an independent measurement of x-ray flux and complement the Bragg crystal measurements by recording the temporal history. An example in Fig. 3 shows that the laser heating produces an immediate onset of L-shell emission, which monotonically grows and peaks near the end of the pulse as predicted by simulations. The measured XRD voltages are converted to spectrally integrated fluxes by an unfold procedure that uses the photocathode sensitivity and experimentally measured frequency distribution. The error, primarily due to the unfold, is $\sim 15\%$. To obtain CE, the XRD signal is integrated over time and divided by the laser energy.

For the series of Xe targets, the CE is 10% with an overall error bar of 30%, which includes a small systematic error between the x-ray spectrometers and diodes. Figure 4 shows the Xe gas and CsI disk data from these experiments, plotting the average values at the median energy of 4.8 keV. For comparison, a compilation of data (0.35 μm laser light only) is also shown. The L-shell solid
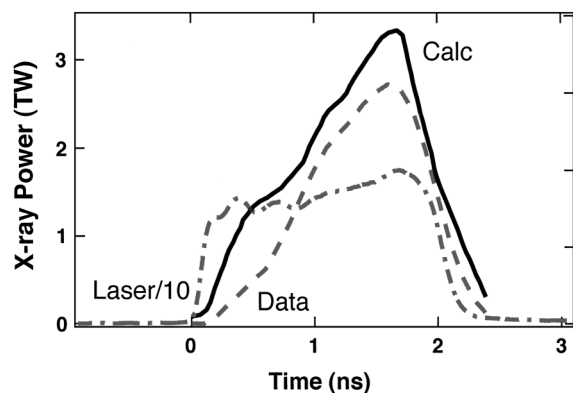
FIG. 3. Total L-shell emission into 4π vs time: data (dashed line) and calculation (solid line). The laser power, divided by a factor of 10 (dot-dashed line), is also shown.

CsI target gives a CE of ~1% and is consistent with past research showing a strong logarithmic decrease with increasing photon energy [4,6,7]. The 10% CE from the supersonically heated Xe-filled targets are nearly $10\times$ above that of CsI and other solid, ablatively driven targets in the same energy range.

Analysis of the 2D time-resolved x-ray images shows the conduction to be efficient enough between the beams to produce a source spatially uniform to 10%. The angular distribution, measured with film packs positioned in the plane defined by the cylindrical axis, was isotropic to within 5% and is consistent with expectations of an optically thin volume emitter.

The experimental T_e can be deduced from temperature-sensitive spectral line intensity ratios. The ratio of the Na-like satellite to the Ne-like resonance line of the $n = 4-2$ transitions has been identified by kinetics modeling of Xe plasmas to decrease with increasing T_e [14]. The ratio for the Xe $n = 4-2$ lines gives values between 0.5 and 0.8 and corresponds to a time-integrated T_e of 4.5–5.5 keV. The Kr spectrum was consistent with this T_e range, but the spectral dispersion was not sufficient for a more precise determination.
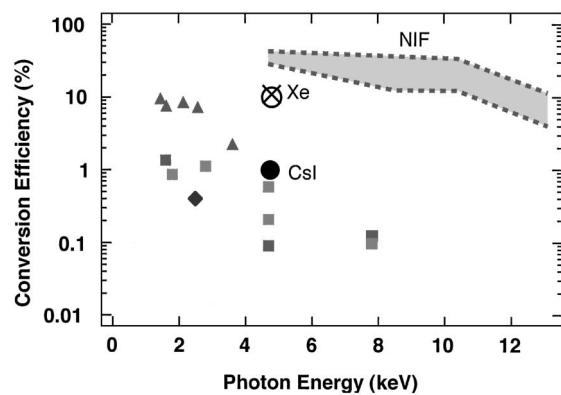
FIG. 4. CE of multi-keV x rays. The solid symbols represent disk data noted in the text: K shell (squares), L shell (diamond), and M shell (triangles). The open circle (data) and cross (2D calculation) are for Xe. The solid circle is for the CsI. The band labeled NIF is the predictions for 60–300 TW of laser power.

A clearer picture of the energetics is provided by simulations summarized in Table I. These compare 1D simulations of cryogenic Xe solid disk target and Xe gas column at 2 ns and do not take into account the dynamics due to the 3D enclosure around the gas. For the gas target, nearly 50% of the energy is thermal (column 1), producing a CE of 20% into >4 keV x rays (column 4). Meanwhile, for the disk target, only 30% is in thermal energy, leading to only 6% in >4 keV radiation. Based on the increased kinetic energy of the disk, we deduce that the laser energy preferentially ionizes the gas as opposed to setting up pressure gradients as in the disk target. The third column shows that the parasitic sub-keV x-ray fraction in the gas is significantly reduced relative to the disk. This reduction is due to the absence of the ablatively created high density, cooler plasma which leads to higher electron conductivity losses in the disk target radiators. In fact, simulations show that, when the density is high enough to produce a subsonic heat front ($>0.2n_c$), the CE significantly drops. Full 2D radiative-hydrodynamic calculations predict a CE of 11% for the Xe targets.

A qualitative understanding of the target behavior can be obtained by examining analytic equations. The plasma is predominantly heated by a supersonic heat wave [15], where the laser energy deposition can be assumed to occur within a volume defined by the diameter of the laser beam and the inverse bremsstrahlung absorption length, ℓ [16]. However, the cooling is determined by radiative and electron conductive losses.

The radiated power can be estimated by a coronal model in which the rate of collisional excitation from the ground state, n_eC, is balanced by the spontaneous radiative decay rate, A. In a simple two-level description where n_u is the upper state population, n_0 is the ground state population, $h\nu$ is the energy of the transition, and all ions are in the average state of ionization, $\langle Z \rangle$, we have $n_uAh\nu \approx n_0n_eC_{u0}h\nu$ and $n_0 \approx n_e/\langle Z \rangle$. If we assume that the power density of the entire L shell is due to the Ne-like ions, then the radiation emitted in TW/cm³ is

$$P_{L\text{-shell}} \approx \frac{n_e^2}{\langle Z \rangle}\left[8.1 \times 10^{-38}F \frac{\exp(\frac{-h\nu}{T_e})}{\sqrt{T_e}} \right], \quad (1)$$

where $F = \sum f_u g_u$ is an averaged oscillator strength weighted by the individual oscillator strengths, f_u, and Gaunt factors, g_u, summed over all species. Non-LTE radiative-hydrodynamic calculations performed to assess the validity of this representation found it to be accurate for temperatures and densities in these experiments. Simulations to determine the parameter, F, using both average

TABLE I. Partition of energy in 1D simulations of a Xe gas column and a cryogenic Xe solid disk target.

	Thermal $1.5nkT_e$	Kinetic $0.5m_ev_e^2 + 0.5m_iv_i^2$	<4 keV x rays	>4 keV x rays
Gas	46%	12%	22%	20%
Solid	29%	28%	37%	6%

atom and detailed calculations, give a fit of $F = 2.5$ for $n_e = 1 \times 10^{21}$ cm^{-3} and $\langle Z \rangle = 44$ with F varying weakly for plasma parameters in the range of interest. Therefore, for the measured average $T_e = 5$ keV, Eq. (1) gives $P_{L\text{-shell}} \sim 800$ TW/cm^3. For this size target, this corresponds to ~ 4 TW, or 20% of the laser power. This provides a reasonable estimate, but will tend to overestimate the CE because the instantaneous power ratio does not take into account the time-dependent ionization and temperature history.

By contrast, the cooling due to electron conduction is much larger. For convenience, we use Spitzer-Harm, where the conduction is proportional to ∇T [17]; flux-limited electron conduction equations give the same order of magnitude loss for these experimental conditions. Here, we assume a model plasma T_e that drops a factor of 2 from the center to the outer radius, R, of the laser channel, $\nabla T_e = T_e/(2R)$. For a cylindrical area $2\pi R \Delta X$ and volume $\pi R^2 \Delta X = A_L \Delta X$, the power lost in TW/cm^3 is

$$P_e = 116 \frac{T_e^{7/2}}{Z \ln \Lambda A_L}, \quad (2)$$

where T_e is in keV, Z is the ionic charge, and $\ln \Lambda$ is ~ 8 for these plasmas. Equation (2) with $R \approx 500$ μm yields 40 TW lost by conduction, comparable to the input. Thus the bulk of the cooling is through electron conductivity and not radiative cooling.

Of note for future extrapolations, we can derive the following analytic equation for T_e if we ignore the radiative losses. By setting the input laser power density equal to electron conduction losses only, Eq. (2) gives

$$T_e = \left[\frac{(\frac{n_e}{n_c})^2}{65 \lambda_L^2} \frac{(Z \ln \Lambda)^2 P_L}{\sqrt{1 - (\frac{n_e}{n_c})}} \right]^{0.2}. \quad (3)$$

In general, Z is temperature dependent [18] but, for these plasma conditions, its dependence is weak. For the experimental conditions, i.e., $P_L = 17.8$ TW, $n_e/n_c = 0.1$, and average charge Z of 44, this equation yields a T_e of 4.9 keV, in good agreement with data. Even if the radiative losses were comparable to the conduction losses, the T_e would only be a factor of $(1/2)^{0.2}$, or 13% lower. Therefore, this model can provide reasonable T_e estimates for high-Z plasmas.

At future facilities such as NIF, the $25\times$ larger laser power could be distributed to produce 25 modular targets at the same size and the same T_e. Alternatively, by inspection of Eq. (3), NIF could heat the same size target to $2\times$ higher T_e and, from Eq. (1), get similar CE at twice the photon energy (e.g., L-shell emission at 10 keV from underdense Ta).

The band labeled NIF in Fig. 4 shows predictions for multi-keV underdense radiators created with 0.35 μm laser light. The upper limit is determined from calculations using 300 TW of laser power for 6 ns into a 7 mm diameter spherical target. The lower limit assumes 60 TW for 2 ns using a 2-mm-diameter, 2-mm-long cylindrical target. Based on weighted averages over the shell emission, they span L-shell (Xe 4.5 keV, Dy 8.6 keV) and K-shell (Cu 8.5 keV, Ge 10.3 keV, and Kr 13.3 keV) emitters. Further development of underdense targets created from gas-filled targets, exploding foil targets, gas jets, or preformed capillary discharge plasmas is a promising way to meet the needs for ever more penetrating backlights and brighter large-area x-ray sources.

[1] As examples, see A. Loveridge-Smith *et al.,* Phys. Rev. Lett. **86**, 2349 (2001); C. Deeney *et al.,* J. Radiat. Eff. **17**, 95 (1999); S. G. Glendinning *et al.,* Phys. Plasmas **7**, 2033 (2000); N. Woolsey *et al.,* Rev. Sci. Instrum. **69**, 418 (1998); F. Ze *et al.,* J. Appl. Phys. **66**, 1937 (1989); D. Phillion *et al.,* Rev. Sci. Instrum. **59**, 1476 (1988).

[2] C. E. Max, C. F. McKee, and W. C. Mead, Phys. Fluids **23**, 1620 (1980).

[3] R. Sigel *et al.,* Phys. Fluids B **2**, 199 (1989), and references therein.

[4] R. L. Kauffman, in *Handbook of Plasma Physics,* edited by A. M. Rubenchik and S. Witkowski (Elsevier, Amsterdam, 1991), Vol. 3, pp. 111–162, and references therein.

[5] R. Pakula and R. Sigel, Phys. Fluids **28**, 232 (1985).

[6] B. Yaakobi *et al.,* Opt. Commun. **38**, 196 (1981); D. L. Matthews *et al.,* J. Appl. Phys. **54**, 4260 (1983); R. Kodama *et al.,* J. Appl. Phys. **59**, 3050 (1986).

[7] D. Phillion and C. J. Hailey, Phys. Rev. A **34**, 4886 (1986).

[8] O. Landen *et al.,* Rev. Sci. Instrum. **72**, 627 (2001).

[9] J. F. Davis *et al.,* J. Radiat. Eff. **17**, 103 (1999).

[10] R. K. Kirkwood *et al.,* Phys. Rev. E **77**, 2706 (1996); S. H. Glenzer *et al.,* Phys. Rev. E **55**, 927 (1997).

[11] H. N. Kornblum *et al.,* Rev. Sci. Instrum. **57**, 2179 (1986).

[12] B. L. Henke *et al.,* J. Opt. Soc. Am. B **1**, 828 (1984).

[13] R. L. Kauffman *et al.,* ICF Quarterly Report No. 6 (2), 1996; Lawrence Livermore National Laboratory Report No. UCRL-LR-50021-96-2, 1996; L. J. Suter *et al.,* ICF Quarterly Report No. 6 (3), 1996; Lawrence Livermore National Laboratory, Report No. UCRL-LR-105821-96-3, 1996.

[14] C. J. Keane *et al.,* Phys. Rev. Lett. **72**, 3029 (1994).

[15] J. Denavit and D. W. Phillion, Phys. Plasmas **1**, 1971 (1994).

[16] J. Dawson, P. Kaw, and B. Green, Phys. Fluids **12**, 875 (1969); J. Lindl, *Inertial Confinement Fusion* (Springer-Verlag, New York, 1998), Chaps. 8 and 11.

[17] L. Spitzer, Jr., *Physics of Fully Ionized Gases* (Interscience, New York, 1964); R. Fabbro, C. Max, and E. Fabre, Phys. Fluids **28**, 1463 (1985).

[18] D. E. Post *et al.,* At. Data Nucl. Data Tables **20**, 397 (1977).